AAS 17-451

VOLUME MULTI-SPHERE-MODEL DEVELOPMENT USING ELECTRIC FIELD MATCHING

Gabriel Ingram[*], Joseph Hughes[†], Trevor Bennett[‡], Christine Reilly[§], and Hanspeter Schaub[¶]

Electrostatic modeling of spacecraft has wide-reaching applications such as detumbling space debris in the Geosynchronous Earth Orbit regime before docking or servicing and tugging space debris to graveyard orbits. The viability of electrostatic actuation control applications relies on faster-than-realtime characterziation of the electrostatic interaction. The Volume Multi-Sphere Method (VMSM) seeks the optimal placement and radii of a small number of equipotential spheres to accurately model the electrostatic force and torque on a conducting space object. Current VMSM models tuned using force and torque comparisons with commercially available finite element software are subject to the modeled probe size and numerical errors of the software. This paper investigates fitting of VMSM models to Surface-MSM (SMSM) generated electrical field data, removing modeling dependence on probe geometry while significantly increasing performance and speed. A proposed electric field matching cost function is compared to a force and torque cost function, the inclusion of a self-capacitance constraint is explored and 4 degree-of-freedom VMSM models generated using electric field matching are investigated. The resulting E-field based VMSM development framework is illustrated on a box-shaped hub with a single solar panel. Despite the complex non-symmetric spacecraft geometry, elegantly simple 2-sphere VMSM solutions provide force and torque fits within a few percent.

INTRODUCTION

Electrostatic modeling of spacecraft and space debris is currently an active area of research with applications in Space Situational Awareness (SSA), Lorentz Augmented Orbits (LAO) and touchless interaction between spacecraft. Spacecraft and debris in both Low Earth Orbit (LEO) and Geosynchronous Earth Orbit (GEO) can become charged by interactions with ambient plasma to such an extent that they are perturbed by Earth's electric and magnetic fields.[1,2] Although accelerations caused directly by Lorentz forces are small in both LEO and GEO, electromagnetic influence on attitude can cause variation in more prominent attitude-dependent perturbations–such as solar radiation pressure–that lead to significant changes in orbital parameters in a matter of hours.[2,3] Objects that are particularly affected by this phenomenon are those with high area-to-mass ratios,

[*]Graduate Research Assistant, Aerospace Engineering Sciences, University of Colorado, Boulder, CO, USA.
[†]Graduate Research Assistant, Aerospace Engineering Sciences, University of Colorado, Boulder, CO, USA.
[‡]Graduate Research Assistant, Aerospace Engineering Sciences, University of Colorado, Boulder, CO, USA.
[§]Undergraduate Researcher, Aerospace Engineering Sciences, University of Colorado, Boulder, CO, USA.
[¶]Alfred T. and Betty E. Look Professor of Engineering, Associate Chair of Graduate Affairs, Department of Aerospace Engineering Sciences, University of Colorado, 431 UCB, Colorado Center for Astrodynamics Research, Boulder, CO 80309-0431. AAS Fellow

HAMR objects, which constitute part of the debris population.[3,4] Improvements in satellite propagation and orbit determination of these debris objects requires electrostatic modeling of some form. Computational efficiency is desirable in both trajectory propagation, and orbit determination.

In addition to natural orbit evolutions, when spacecraft or debris charges are controlled artificially using ion or electron beams, both Lorentz and Coulomb forces can be harnessed for useful purposes, such as LAO, active debris removal and touchless de-tumbling of spacecraft.[5–7] LAO applications are varied, and include drag compensation in elliptical orbits, inclination control, and rendezvous.[5] In addition, Lorentz forces can be used to augment formation flying reconfiguration control laws to reduce thruster ΔV requirements, and for limited propellentless propulsion.[8–10]

While LAO exploit the Lorentz force experienced by spacecraft moving quickly through a magnetic field, Coulomb forces between spacecraft and debris can also be utilized. Electrostatic tugging is proposed as a means of active debris removal and for applications in formation flying.[6,11,12] The Geosynchronous Large Debris Reorbiter (GLiDeR) is one active debris removal concept that harnesses these electrostatic effects. The GLiDeR remotely charges a defunct satellite or piece of space debris with an electron beam, allowing it to interact with the object for the purposes of changing the object's orbit. Orbit raising of 250 km can be accomplished in a little over two months using Coulomb interaction between GLiDeR and a target.[13] Electrostatic de-tumbling of space objects is currently being researched, and shows promise as a method for reducing debris tumbling rates to within an acceptable magnitude for grappling in servicing missions.[7,14–16]

Many of these applications motivate and require faster-than-realtime methods of electrostatic modeling. Although finite element method (FEM) software, such as ANSYS Maxwell 3D©, provide accurate results, calculations of the force and torque between a target and command spacecraft at one relative position and orientation requires time on the order of minutes. The duration of this calculation is unacceptable for control purposes. The Multi-Sphere Method (MSM) is a lower-fidelity electrostatic modeling technique that can be evaluated quickly enough for faster-than-realtime applications.[17,18]

MSM is an elastance-based method for predicting the force and torque on conductors.[19] It is similar to the method of moments in its linear form,[20] but differs in that the size and location of the nodes are hand-tuned rather than derived from first principles. This tuning is done by an optimizer to match force and torque which are computed using a high-fidelity FEM software. Because of this, MSM can predict Coulomb forces and torques very quickly at accuracies of 1-2%. Recent work largely automates the process of generating MSM models using local optimizers; however, challenges to current MSM model generation methodologies remain.[1] In particular, current automation of Volume-MSM (VMSM) modeling is accomplished by fitting to FEM generated force and torque data. Not only is the process of generating FEM data time consuming, but it is prone to producing noisy data in the far from the target model. The effect of noisy data is mitigated by fitting to near-field data and imposing a self-capacitance constraint upon the optimization process. In addition, fitting to force and torque data ties VMSM modeling methodologies to a specific probe geometry.

This paper introduces a novel automated method of generating VMSM models by matching the electric field in the vicinity of the target rather than Coulomb forces and torques. Since the electric field data is produced using Surface-MSM (SMSM), it is much smoother in the far field, which avoids many of the drawbacks of current MSM model generation techniques. E-field fitting greatly reduces the time required to generate a VMSM model while maintaining the model accuracy associated with current modeling techniques. The E-field matching method can also be demonstrated

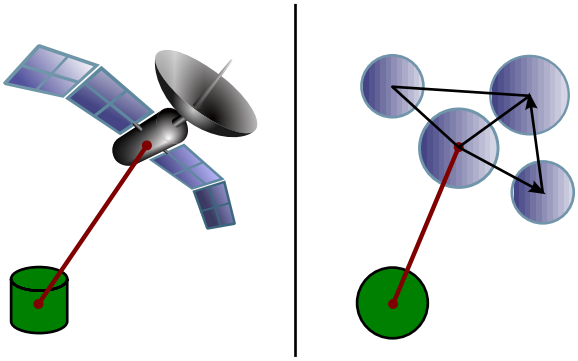

Figure 1. Illustration of the MSM Concept[18]

to allow for creation of 4 degree-of-freedom VMSM models.

A brief review of the Multi-Sphere method is presented. The optimizer cost functions for current VMSM and E-field matching model generation methodologies are compared near a solution. Force and torque model accuracies when the E-field matching method is applied to a complex asymmetric box-and-panel geometry, with and without a self-capacitance constraint, are investigated. The computational effort of producing one, two and three-sphere VMSM models of the box-and-panel geometry is detailed. The effect of data reduction on model accuracy when a self-capacitance constraint is imposed is shown, and a comparison between the accuracies of reduced-coordinate and 4 degree-of-freedom models is made.

MULTI-SPHERE METHOD BACKGROUND

MSM provides a reasonably accurate model of a spacecraft's electrostatic properties for applications that require faster-than-realtime results. MSM solves for the force and torque on a conductor by first finding the charge on a number of virtual spheres placed within the body. The charge on the spheres is found by assuming all spheres are equipotential and solving a linear system. MSM divides into VMSM, which uses a small number of spheres placed within the volume of the conductor, and SMSM, which places a large number of spheres on the surface of the conductor. It is more difficult to generate VMSM models because the size and location of the spheres must be found using an optimizer; however, VMSM models are much faster to run once completed. SMSM models are easier to set up because the sphere locations are specified, and the sphere size can be found by matching self capacitance, which is computed from commercial FEM software. Generally, SMSM models show higher accuracy when compared to FEM-generated force and torque data.[4] Although SMSM greatly reduces the effort required to create a MSM model for a given spacecraft geometry and increases the accuracy of the model, it comes at increased computational cost at runtime due to the large number of spheres.

Both the Volume Multi-Sphere Method and Surface Multi-Sphere method represent an conducting object as N spheres, as shown in Figure 1. These methods only differ in the number, size and placement of the spheres used to represent the conductor. The MSM formulation currently assumes that the surface of the target craft or debris is perfectly conducting, which implies that all MSM spheres within a body are equipotential.

Thus, the charge on each sphere in a MSM model, which may include multiple distinct spheres

outside of the target model, is only a function of the sizes of the spheres in the complete model and their relative positions. Letting N_T be the total number of MSM spheres in a MSM model, computed as the sum of the number of spheres in the target model and the number of spheres outside the target model, all MSM spheres can approximated as point charges. The $N_T \times 1$ charge matrix, $\mathbf{q} = \begin{bmatrix} q_1 & q_2 & \dots & q_{N_T} \end{bmatrix}^T$, which contains the charge on each sphere of a MSM model, is related to the $N_T \times 1$ sphere voltage matrix $\mathbf{V} = \begin{bmatrix} V_1 & V_2 & \dots & V_{N_T} \end{bmatrix}^T$ through Eq. (1)[17]

$$\mathbf{q} = \frac{1}{k_\mathrm{c}} \left[C_\mathrm{M} \right] \mathbf{V} \tag{1}$$

where k_c is the Coulomb constant, and the $N_T \times N_T$ matrix $[C_M]$ is the Position Dependent Capacitance (PDC) matrix. For a general N_T sphere MSM model, the PDC matrix is difficult to produce; however, its inverse, the elastance matrix $[S]$, contains only functions of the sphere radii R_i and relative distances between spheres $r_{i,j}$. $[S]$ is formulated as shown in Eq. (2)[19]

$$[S] = \begin{bmatrix} \frac{1}{R_1} & \frac{1}{r_{1,2}} & \dots & \frac{1}{r_{1,N}} \\ \frac{1}{r_{2,1}} & \frac{1}{R_2} & \dots & \frac{1}{r_{2,N}} \\ \vdots & \vdots & \ddots & \vdots \\ \frac{1}{r_{N,1}} & \frac{1}{r_{N,2}} & \dots & \frac{1}{R_N} \end{bmatrix} \tag{2}$$

The charges, which lead to the force and torque, are found by solving the linear system. For an isolated conductor with a small number of spheres this can be done analytically, but in the majority of cases is is done numerically. This computation is expensive, and is the cause of decreased run-time performance when using the SMSM method.

The charge set $\mathbf{q}$ is calculated using Eq. (1). The charges, q_i, are used to calculate the electric field produced by the model, and forces and torques that an object model experiences subject to one or more external point charges. Denoting the position vector of an external point charge as $\mathbf{r}_k$ and the relative position vector of each MSM model sphere with respect to its center of mass as $\mathbf{r}_i$, the force, $\mathbf{F}$, and torque, $\mathbf{T}_\mathrm{O}$, applied to the target model about its center of mass by all external spheres with charges q_k are given in Eqs. (3) and (4)[18]

$$\mathbf{F} = -k_\mathrm{c} \sum_{k=1}^{M} q_k \sum_{i=1}^{N} \frac{q_i}{||\mathbf{r}_{i,k}||^3} \mathbf{r}_{i,k} \tag{3}$$

$$\mathbf{T}_\mathrm{O} = -k_\mathrm{c} \sum_{k=1}^{M} q_k \sum_{i=1}^{N} \frac{q_i}{||\mathbf{r}_{i,k}||^3} \mathbf{r}_i \times \mathbf{r}_{i,k} \tag{4}$$

where $\mathbf{r}_{i,k}$ is the relative position of the k^{th} external sphere with respect to the i^{th} internal MSM sphere. N is the total number of spheres in the target model, and M is the total number of spheres external to the target. Adding arbitrary numbers of external spheres does not add to the complexity of MSM modeling because they can be appended to the charge and elastance matricies; however, doing so will increase computational burden. Whole MSM models can be appended when the calculation of force and torque between two complex geometries is desired.

The electric field at any point exterior to the spheres of a MSM model is given by the superposition

of the electric fields of each sphere, as shown in Eq. (5)

$$\mathbf{E} = k_{\mathrm{c}} \sum_{i=1}^{N_T} \frac{q_i}{||\mathbf{r}_{i,l}||^3} \mathbf{r}_{i,l} \tag{5}$$

where l is a point of interest in the space outside of the MSM model spheres, and $\mathbf{r}_{i,l}$ is the relative position between the i-th MSM model sphere and l.

Current VMSM model fitting methods minimize a cost function based upon the difference between the force and torque vectors predicted by a VMSM model and the force and torque vectors generated by commercial FEM software. One such cost function is given by Eq. (6)[1]

$$J = \frac{100}{L} \left(\sum_{l=1}^{L} \frac{||\mathbf{F}_{\mathrm{VMSM},l} - \mathbf{F}_{\mathrm{FEM},l}||}{||\mathbf{F}_{\mathrm{FEM},l}||} + \frac{||\mathbf{T}_{\mathrm{VMSM},l} - \mathbf{T}_{\mathrm{FEM},l}||}{||\mathbf{T}_{\mathrm{FEM},l}||} \right) \tag{6}$$

To alleviate far-field data noise effects in the optimization process, current methods utilize a self-capacitance constraint. The self-capacitance C of a VMSM model is given by Eq. (7)[1]

$$C = \frac{Q}{V} = \frac{\sum_{i=1}^{N} q_i}{V} = k_{\mathrm{c}} \sum_{i=1}^{N} \sum_{j=1}^{N} (C_{\mathrm{M}})_{ij} \tag{7}$$

ELECTRIC FIELD VMSM MODEL FITTING

SMSM E-field Data Generation

Using the current VMSM methodology, the sphere positions and radii are varied by an optimizer to best match force and torque data produced by a commercial FEM program.[1,17,18] This methodology requires significant hand-tuning of model parameters for a model that fits force and torque data accurately due to noisy FEM data in the far field, dependance on probe size, and convergence properties of the force and torque cost function. Recent work largely streamlines the process of generating VMSM models using ANSYS Maxwell 3D to generate numerical data.[1] The workflow for current VMSM model fitting starts with generating solid models for a target and probe geometry in FEM software and calculating accurate force and torque values between them at many relative positions. Self-capacitance of the target spacecraft is also calculated.

A complete sweep of locations for force and torque matching and validation may take hours and variations in accuracy depend heavily upon how many data points are used. In addition, complicated workarounds that automatically change probe radius are required to get accurate results. Current techniques use a spherical probe which has a radius that is a function of its distance from a target. The dependence on external probe geometry for force and torque calculations is clear in the above force and torque equations. This dependence is included into VMSM model generation when a cost function based on force and torque is used.

The workflow proposed in this paper seeks to address both of these issues. The initial step in modeling is the same — a solid model of the target spacecraft is created. However, a solid model of external probe geometry is optional, and only used to gather limited force and torque data for verification of a model. A target voltage is prescribed and FEM software is used to calculate the self-capacitance of the target.

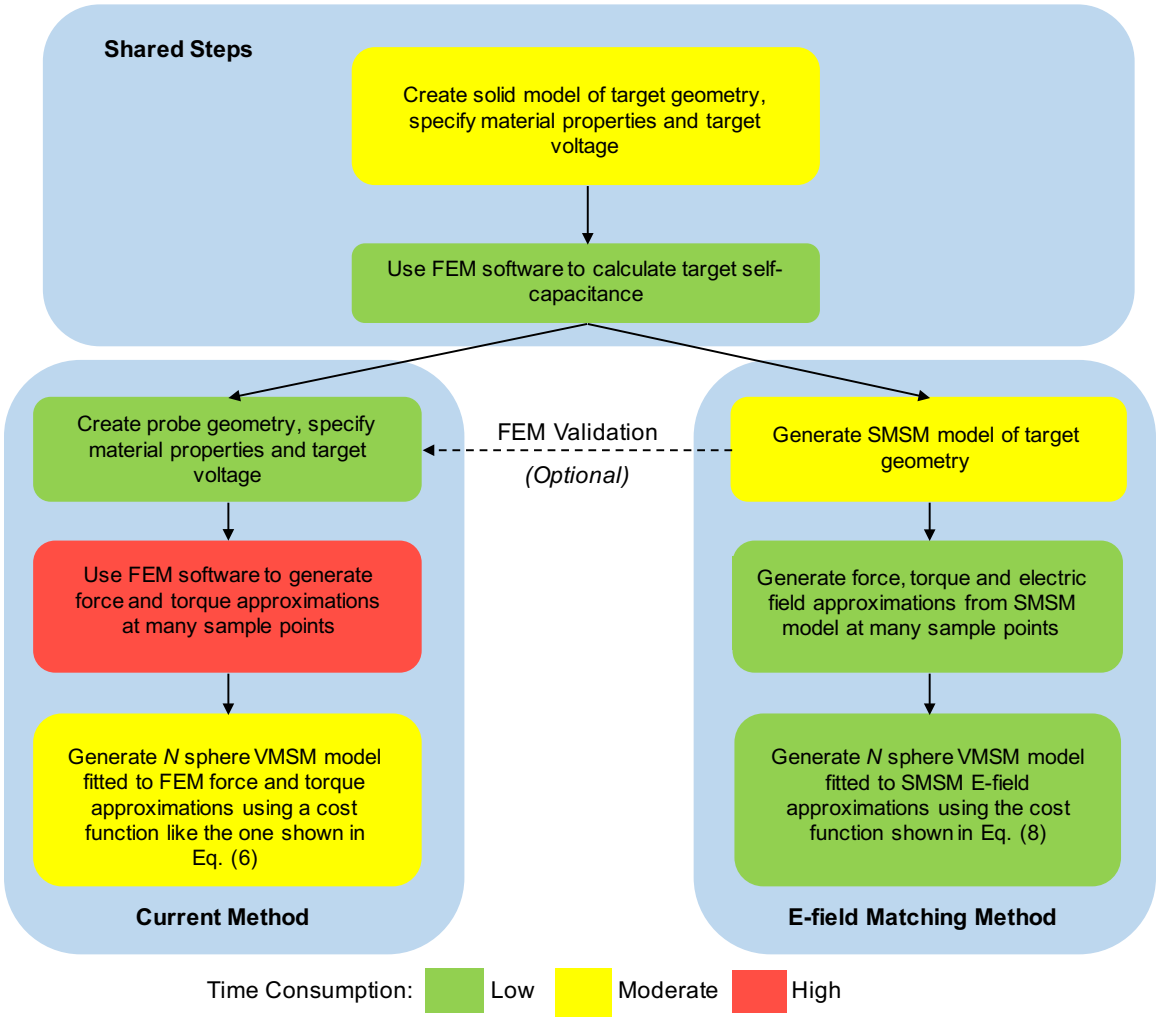

Figure 2. Proposed Workflow Comparison with Previous Force and Torque Methods

A SMSM model of the target geometry is then generated using any appropriate method. One method, appropriate for spherical and cylindrical geometries, is to use a golden spiral algorithm to distribute SMSM spheres on the surface of the geometry.[18] A method appropriate for flat geometries is to use a function like MATLAB's *meshgrid* to generate a distribution of sphere positions on the surface of a plane. This distribution can then be translated, rotated and combined with other planar distributions of spheres to form complex SMSM geometries.[21] When combining distributions, care should be taken to eliminate redundant spheres so that none overlap. Root finders like Matlab's *fsolve* can then be used with Eq. (7) to determine appropriate sphere radii to match the SMSM model self-capacitance to the self-capacitance of the solid model. Using the prescribed target voltage and Eq. (1), the charge on each SMSM sphere is calculated. Using the same equation applied to an N-sphere VMSM model optimization problem, an optimizer is used to select the optimal positions and radii of the model spheres to minimize the following cost function at sample points l

$$J\left(R_1, R_2, \ldots, R_N, \mathbf{r}_1, \mathbf{r}_2, \ldots, \mathbf{r}_N\right) = \sum_{l=1}^{L} \frac{||\mathbf{E}_{VMSM,l} - \mathbf{E}_{SMSM,l}||}{||\mathbf{E}_{SMSM,l}||} \tag{8}$$

where L is the total number of electric field sample points.

Using this cost function results in two major improvements to the prior methodology. The first improvement is the separation of VMSM model generations from any external probe geometry. The second improvement is in the time required to complete all the steps in generating a VMSM model. G II in (Reference 17) shows a comparison of the time required to create a three-sphere VMSM model using force and torque fitting at 82 relative positions. These results indicate that force and torque fitted VMSM models require setup time measured in hours. Although the proposed E-field fitting methodology adds the step of creating a SMSM model for a given target geometry and voltage, this process requires significantly less computational effort than computing forces and torques at many relative positions with FEM. (Reference 1) discusses fitting to much smaller numbers of force and torque data points; however, using the proposed method, hundreds of data points are calculated and used to create a VMSM model in less than the time it requires to calculate one force and torque calculation using commercial FEM software. A flowchart comparing the previous force and torque optimization procedure and the proposed E-field matching method is included in Figure 2.

SMSM Validation

Before optimizing on a cost function built from a SMSM model, it is prudent to compare the accuracy of SMSM to other methods. The Method Of Images (MOI) provides an analytic infinite series solution to the problem of predicting the force between two spherical conductors.[22,23] The method consists of placing smaller and smaller image charges within the body of each sphere to balance out the potential on the surfaces. As the number of image charges increases, the solution converges.

SMSM models of spheres are made with a variable number of spheres, and the force between the two bodies is compared to that predicted by MOI. For this case, two spheres with 1 meter radius are separated by 5 meters, and charged to ± 10 kV. The results are plotted in Fig. 3

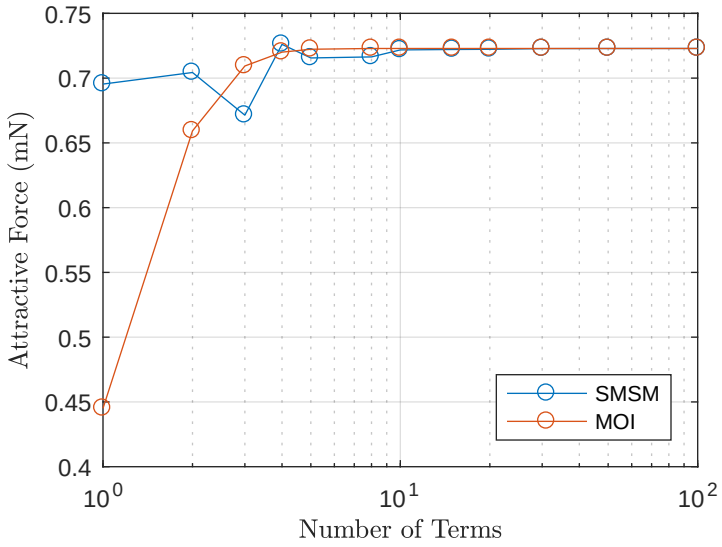

Figure 3. Comparison Between MOI and SMSM

The x-axis indicates either the number of images charges used in each sphere for the MOI, or the

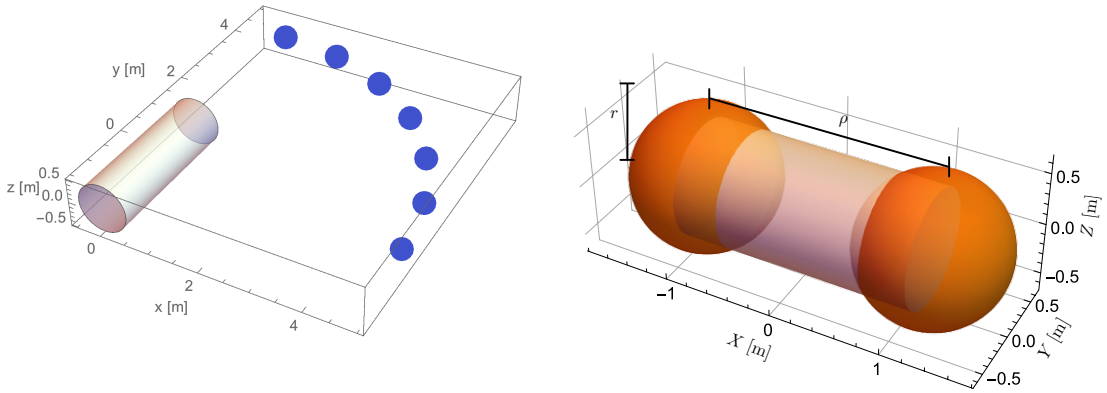

(a) Distribution of Sample Points Around Cylinder

(b) Two-Sphere VMSM Cylinder Model with Parameter Annotations[1]

Figure 4. Cylinder Data Distribution and VMSM Model Parameters

number of individual spheres in each SMSM sphere. The MOI converges with 40 image charges, and SMSM converges with around 100 spheres. Since both methods converge to the same value, SMSM is validated as a method for predicting forces and torques on perfect conductors.

Target Geometry, Data Generation and Optimization Methods

Two target geometries are used to compare the proposed E-field matching method to the previous force and torque method and to establish the accuracy of models generated using E-field matching. A two-sphere VMSM model is created for a charged cylinder, with a radius of 0.5 m and a height of 3 m, centered at the origin and oriented along the y-axis using the E-field matching method. This geometry is selected for easy comparison to previous work using force and torque matching.[1,17,18]

Data for the study involving the cylinder geometry are generated at evenly spaced intervals on 90 degree arcs of circles centered at the origin, lying in the x-y plane and in the fourth quadrant. The symmetry of the cylinder model requires data in only one quadrant for the optimization process. Force and torque data is generated using Maxwell 3D at the selected sample points. A SMSM model of the cylinder, shown in Figure 5, is created to generate E-field data at the same sample points. Only sample points lying on the arc of a 5 m radius circle are used for optimization, as shown in Figure 4(a).

Two optimization methods are used to generate cylinder VMSM models: a global optimization method using Mathematica's Differential Evolution algorithm is used to optimize the force and torque cost function of Eq. (6), and MATLAB's *fmincon* local optimizer is used to minimize the E-field cost function of Eq. (8). Self-capacitance for the cylinder is calculated using Maxwell 3D.

Since a two-sphere VMSM model is used to represent the cylinder and the cylinder has symmetry about the x-axis, the VMSM model can be parameterized by one radius value r, which is shared by both spheres, and the separation distance, ρ, between the two spheres. This model is shown in Figure 4(b).

Using this model, an exact formula for the VMSM model self-capacitance can be derived, as

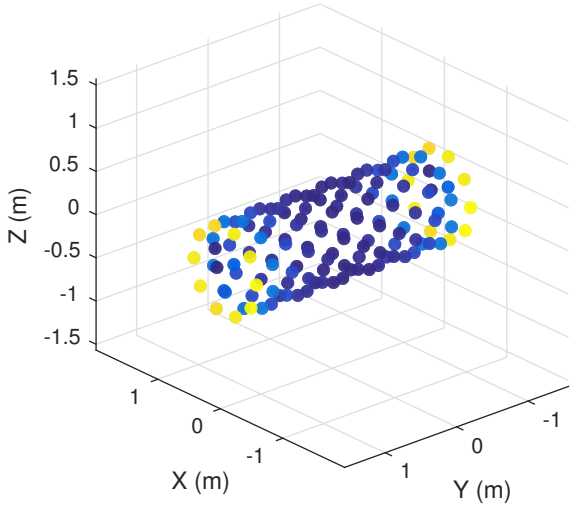

Figure 5. SMSM Model of a Cylinder, Color Indicates Charge

shown in Eq. (9)[1]

$$C = \frac{1}{k_c}\frac{2r\rho}{r+\rho} \tag{9}$$

Imposing a self-capacitance constraint, matching the VMSM model self-capacitance to the value calculated by FEM, ensures that Lorentz forces and far-field Coulomb forces are automatically matched. In addition, it reduces the optimization problem to one dimension, because for any r value there is only one corresponding ρ value for which the constraint is met. Solving Eq. (9) for ρ yields Eq. (10)[1]

$$\rho = \frac{rC_{\text{mod}}}{2r - C_{\text{mod}}} \tag{10}$$

where

$$C_{\text{mod}} = k_c C \tag{11}$$

Since C_{mod} is a scaling of the self-capacitance, it is used to impose the self-capacitance constraint in the following studies because its value is on the order of model parameters. Both the optimal r and ρ values are solved for using *fmincon* and the self-capacitance constraint is imposed numerically.

The second target spacecraft geometry that is selected for this study is a box-and-panel satellite modeled as a cube shaped bus with a long, slender panel attached. The bus width, height and depth are 3 m. The panel width is 3 m, depth is 0.2 m and height is 8.5 m. The panel is located on the top of the bus extending in the z-axis direction with one of its large faces coplanar with the positive y face of the bus. This model geometry is shown in Figure 6. This geometry is selected because it has significant variation from simple geometric shapes like cylinders and represents a realistic target spacecraft. It also shows symmetry that can be used to impose additional constraints on the positions of the VMSM model spheres, and this symmetry is exploited to reduce the amount of data that is required for the optimization procedure.

A SMSM model of the box-and-panel is generated using MATLAB's *meshgrid* feature, and electric field data is generated using Eq. (5), at positions spread radially about the SMSM model. Sample

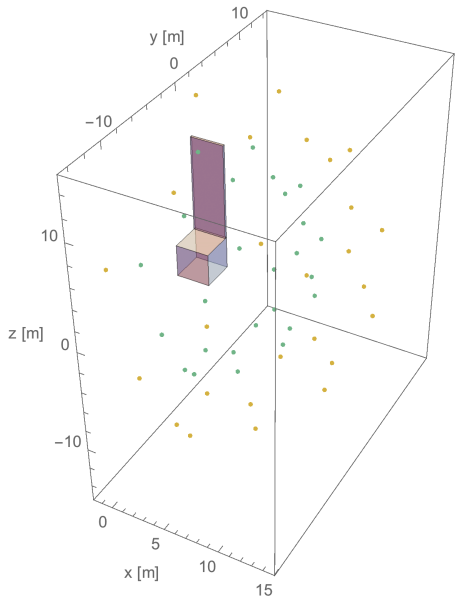

Figure 6. Box-and-Panel Geometry with Data Point Distribution

points are generated using the golden spiral algorithm, which places equally spaced points on the surface of a sphere.[24] This radial spread of electric field data produces distributions of shells of data, which are easily selected or neglected, or reduced to hemispheres or octants for fitting, such as the one shown in Figure 6. Whole spherical shells of data are produced for the box-and-panel geometry; however, due to the symmetry of the model, the complete behavior of the electric field produced by the SMSM model can be captured in one hemisphere of data.

One, two and three-sphere VMSM reduced-coordinate models are created with this data using E-field matching and MATLAB's *fmincon* optimization algorithm. Various sets of data, including whole spheres, hemispheres and multiple shell sets, are used in the optimization processes. In addition, a three-sphere 4 degree-of-freedom VMSM model is generated using E-field matching and *fmincon*. Only shells with radii larger than 12 m are used for optimization to avoid overlap between sample points and SMSM spheres, which would invalidate Eq. (5). Like the cylinder model optimization process, the box-and-panel self-capacitance is calculated using Maxwell 3D and the self-capacitance constraints on the optimization processes are imposed numerically. Additional inequality constraints are imposed for the two and three-sphere VMSM models to ensure aesthetically pleasing models in which spheres do not overlap.

COST FUNCTION COMPARISON

The cost function of Eq. (6) is compared with the proposed electric field cost function of Eq. (8) to compare their characteristics. Both cost functions are used to generate two-sphere VMSM models for a perfectly conducting cylinder charged to 30 kV. Maxwell 3D is used to determine a cylinder self-capacitance value of 106.8345 pF. Noting a potential singularity in Eq. (10) when r is one half C_{mod}, the cost function values, shown in Figures 7(a) and 7(b), along the intersection with the self-capacitance constraint surface are plotted against r for which ρ is positive. The r values minimizing both cost functions are nearly identical, differing by only 0.2%. Investigating the cost

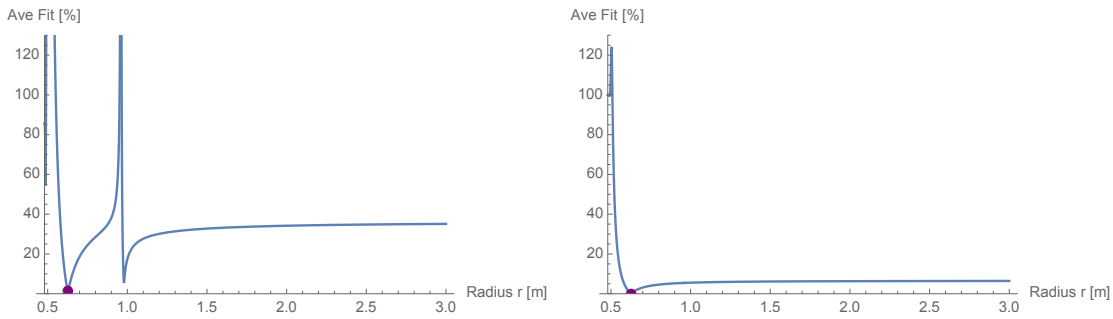

(a) Former Force and Torque Cost Function

(b) New E-field Cost Function

Figure 7. Force and Torque and E-field Cost Functions for Cylinder Model

function sensitivities near both minima suggests that force and torque errors are more sensitive to model parameters than E-field errors are. The proposed E-field cost function shows desirable characteristics, particularly for a local optimization algorithm like *fmincon*. It is generally smooth when compared with the force and torque cost function, and apart from a small region near the singularity in ρ, approaches its minimum unimpeded.

CONSTRAINED AND UNCONSTRAINED BOX-AND-PANEL VMSM MODELS

One, two and three-sphere box-and-panel VMSM models are generated with and without a self-capacitance constraint in order to determine the usefulness of the constraint when applied to an optimization problem without far-field data noise. Models are fit to data in three whole spherical shells with radii of 15, 20 and 25 m. Symmetry of the box-and-panel geometry about the $y-z$ plane is used to reduce the $4N$ degree-of-freedom optimization problem to a $3N$ degree-of-freedom problem. Imposing a self-capacitance constraint reduces the degrees-of-freedom to $3N-1$. The model is charged to 30 kV. Maxwell 3D is once again used to calculate self-capacitance, and returns a value of 336.14 pF. Optimizer initial conditions are chosen loosely based on the box-and-panel geometry. A visualization the VMSM models of the box-and-panel geometry is included in Figure 8. Tables 1-3 show the initial and final conditions for the one, two and three-sphere box-and-panel models, with and without the self-capacitance constraint.

Table 1. Initial and Final States for One-Sphere VMSM Model Optimization, C- Constrained, NC-Non-Constrained

	R_1 [m]	y_1 [m]	z_1 [m]
Initial	1.000	0.000	0.000
Final C	3.021	0.626	2.914
Final NC	2.951	0.608	2.785

Shell-averaged force and torque errors of the six VMSM models with respect to the SMSM generated data are shown in Figures 9(a) and 9(b), respectively. As can be seen, the self-capacitance constraint has utility even when far-field noise is not a concern. In particular, when generating a one-sphere model the self-capacitance constraint ensures that force errors far from the target geometry continue to decay as sample point radius is increased. The effect of the self-capacitance constraint

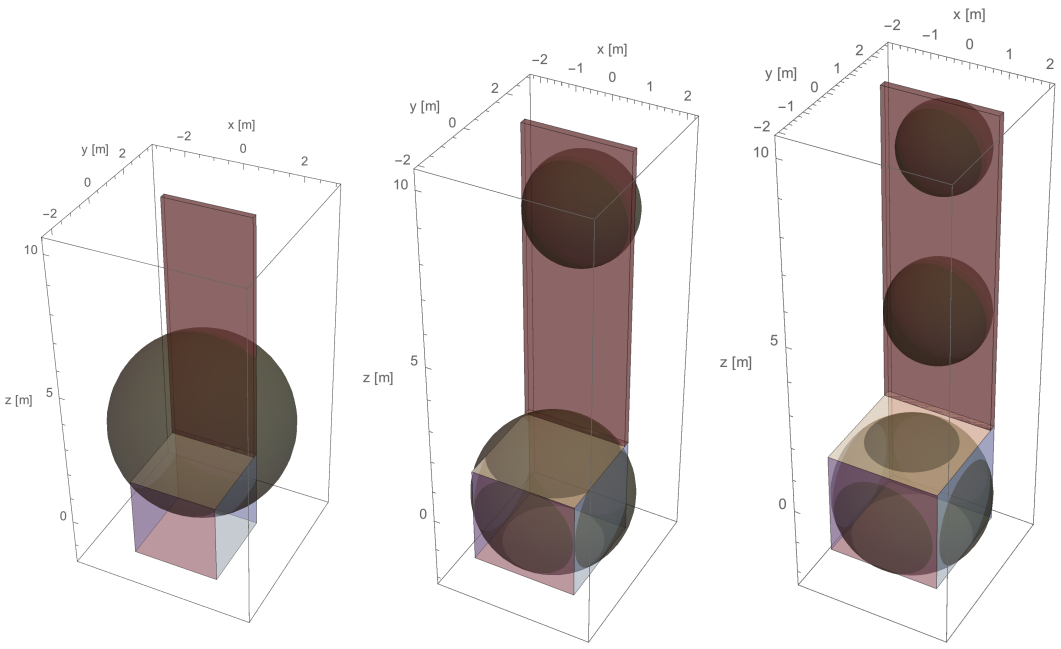

(a) One-Sphere Model (b) Two-Sphere Model (c) Three-Sphere Model

Figure 8. Visualizations of VMSM Box-and-Panel Geometry Models

Table 2. Initial and Final States for Two-Sphere VMSM Model Optimization, C- Constrained, NC- Non-Constrained

	R_1 [m]	R_2 [m]	y_1 [m]	z_1 [m]	y_2 [m]	z_2 [m]
Initial	1.000	1.000	0.000	0.000	1.400	6.000
Final C	2.202	1.458	0.135	0.210	1.596	8.183
Final NC	2.201	1.471	0.134	0.207	1.600	8.177

Table 3. Initial and Final States for Three-Sphere VMSM Model Optimization, C- Constrained, NC- Non-Constrained

	R_1 [m]	R_2 [m]	R_3 [m]	y_1 [m]	z_1 [m]	y_2 [m]	z_2 [m]	y_3 [m]	z_3 [m]
Initial	1.000	1.000	1.000	0.000	0.000	1.400	6.000	1.400	9.000
Final C	2.039	1.323	1.120	-0.008	-0.166	1.319	4.584	1.555	8.972
Final NC	2.041	1.322	1.119	-0.007	-0.163	1.321	4.612	1.556	8.974

is also dramatic for the two-sphere model. The force errors of the two and three-sphere models are nearly identical at 30 m from the target geometry when the constraint is imposed, whereas without it the two-sphere model model force errors remain significantly larger than the three-sphere model's. It is interesting to note that, as more spheres are added to the VMSM model, self-capacitance is matched automatically as displayed by the three-sphere force and torque errors. Both the constrained and non-constrained model errors overlap, and the optimal model parameters of each are nearly identical.

Another benefit of imposing the self-capacitance constraint is that it can significantly reduce

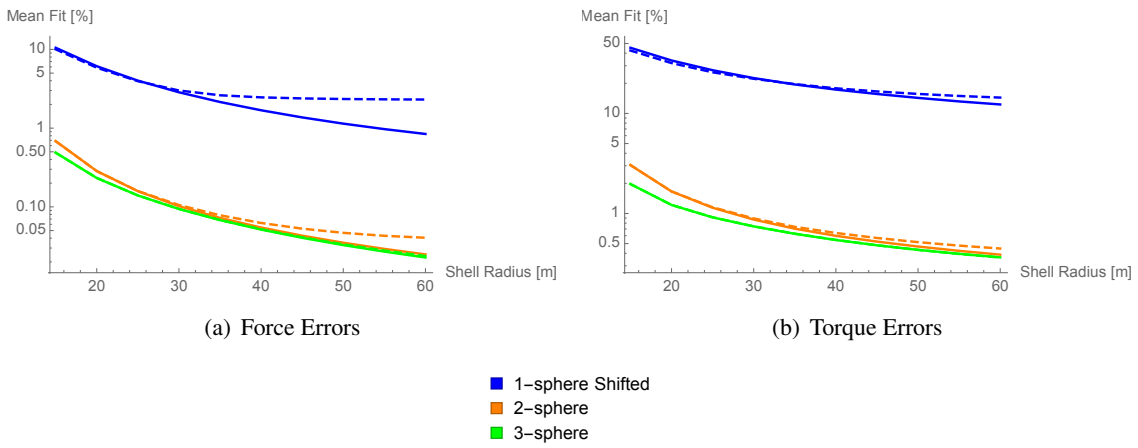

(a) Force Errors

(b) Torque Errors

Figure 9. VMSM Model Errors with Respect to SMSM Data, (—) Constrained, (- -) Non-Constrained

computational effort. The number of function calls required to generate each of the six models is recorded. The results are shown in Figure 10. The results show that imposing the self-capacitance constraint consistently results in increased performance regardless of how many sphere are used to create the VMSM model. This performance increase is due to the reduced dimension of the search space when a self-capacitance constraint is enforced. Given the increased force and torque accuracy and decreased computation effort, the self-capacitance constraint should be enforced even when far-field noise is not a concern.

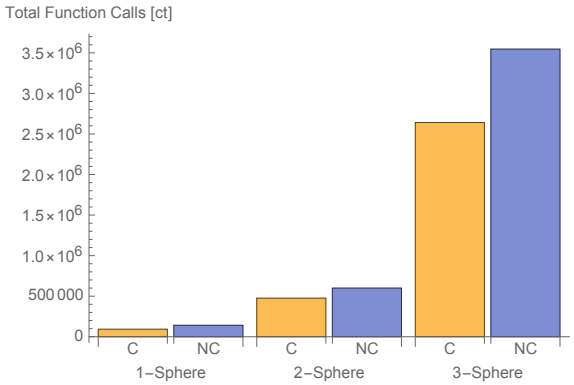

Figure 10. Total Function Calls Required to Generate One, Two and Three-Sphere Box-and-Panel VMSM Models

REDUCED-SHELL DATA SETS WITH SELF-CAPACITANCE CONSTRAINT

Since imposing a self-capacitance constraint forces force vectors in the far-field to automatically match, it is desired to investigate whether or not fewer numbers of shells with smaller radii can be used to effectively generate VMSM models. This question is interesting for two reasons: smaller data sets will reduce the amount of time required for optimization, and fitting to data closer to the target might increase near-field accuracy without significantly affecting accuracy at larger distances.

A three-sphere VMSM model is used to model the box-and-panel geometry. The VMSM model

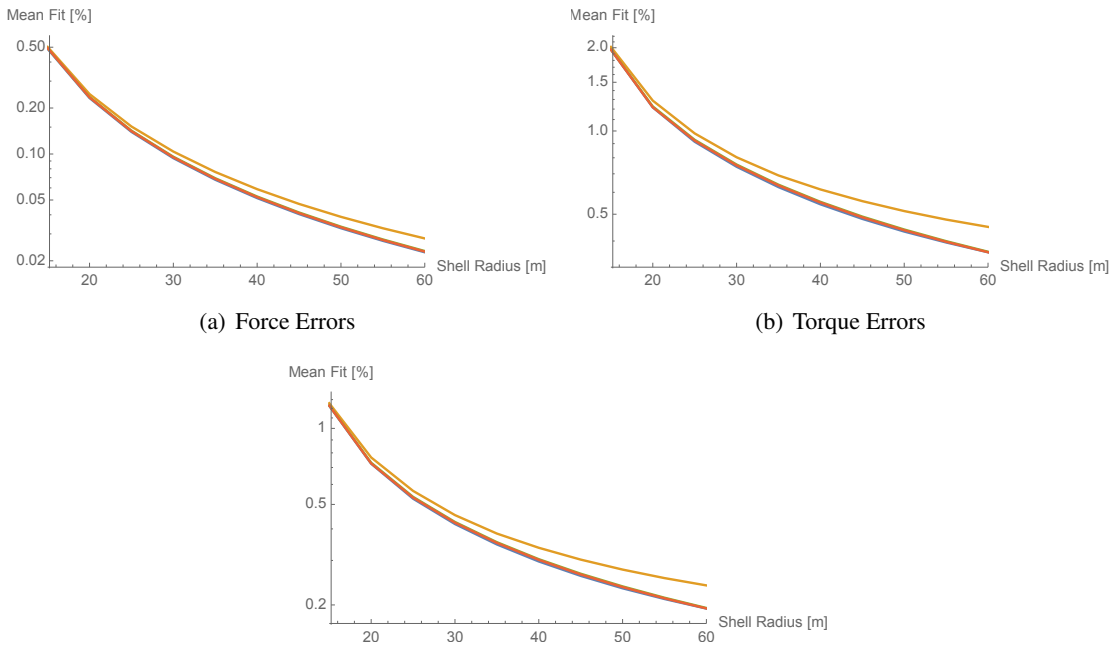

(a) Force Errors

(b) Torque Errors

(c) Average Errors

Figure 11. Shell-Reduction Three-Sphere VMSM Model Errors, (—) 3 Whole Shells, (—) 15 m Shell, (—), 14m Shell, (—) 12 m Shell

is fit to single shells at radii of 12, 14 and 15 m. The model voltage is set to 30 kV, and a self-capacitance constraint of 336.14 pF is imposed. The accuracy of these models are compared with each other and to the three-sphere constrained model generated using three whole shells. The resulting shell-averaged force, torque, and average error plots when compared with the SMSM model are shown in Figures 11(a)-11(c). These results show negligible differences in force and torque accuracy near the target, while the model fitted to the 12 m radius shell shows degraded accuracy far from the target. Accuracies of models fit to three whole shells and to 14 m and 15 m shell radii are nearly identical. The practical impact of the degraded accuracy for the model fitted to the 12 m shell is very small; however, for high accuracy at large distances from a target, a model should be fitted to at least one shell with a larger radius.

The performance impact of reducing the number of shells is analyzed by recording the number of function calls required to generate each model. The results are shown in Figure 12. These results show that there is not a significant gain in performance from just reducing the number of shells used in the optimization process; however, a significant gain does arise when using single shells closer to the target geometry. The number of function calls required to generate a three-sphere VMSM model of the box-and-panel using a single 12 m shell is significantly less than half the number of function calls required to generate the same model using a single 15 m shell or 3 shells. The performance increase comes with degraded accuracy at large distances, so the requirements of the model must be considered before using shell reduction.

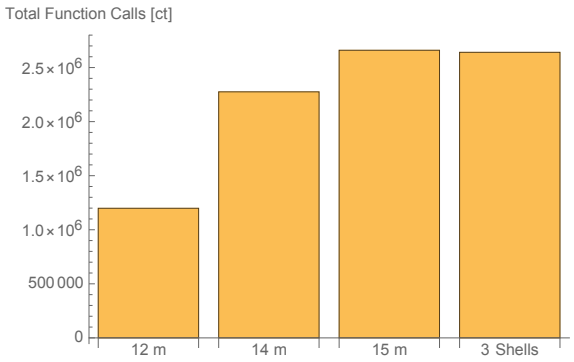

Figure 12. Total Function Calls for Three-Sphere Models Generated with Shell Reduction

Table 4. Initial and Final States for Three-Sphere 4DOF VMSM Model Optimization

	Initial	Final
R_1 [m]	1.000	2.051
R_2 [m]	1.000	1.299
R_3 [m]	1.000	1.106
x_1 [m]	0.000	-0.004
y_1 [m]	0.000	-0.004
z_1 [m]	0.000	-0.136
x_2 [m]	0.000	0.038
y_2 [m]	1.400	1.385
z_2 [m]	6.000	4.788
x_3 [m]	0.000	-0.028
y_3 [m]	1.400	1.534
z_3 [m]	9.000	8.993

MODELING USING GENERAL 4 DEGREE-OF-FREEDOM MSM SPHERES

Previous work focuses on simple geometries that have high levels of symmetry, like the cylinder model. For geometries like these, the number of MSM optimization parameters can be reduced significantly by specifying, for example, that the cylinder MSM spheres must lie on the symmetry axis. As geometric complexity increases, so does the effort required to find symmetries to exploit and analytically parameterize them. Using general MSM 4 degree-of-freedom (4DOF) modeling allows each MSM sphere to have 3 location and one radius degree of freedom. This avoids the need to find symmetry and allows for optimization in a $4N$ dimension search space. Each parameter associated with a VMSM model sphere is found through optimization, and the up-front human-involvement cost of generating a model is reduced.

A three-sphere VMSM model of the box-and-panel geometry is generated using data in shells with radii of 15, 20 and 25 m. A self-capacitance constraint is enforced using a value of 336.14 pF. The model voltage is set to 30 kV. The initial conditions for the 4DOF fitting problem are shown in Table 4. The force and torque accuracy of the 4DOF model with respect to the box-and-panel SMSM model is compared to three-sphere 3DOF models using three whole shells and one half shell at 15 m in Figures 13(a) and 13(b). The model with the least accuracy is the 3DOF model fitted

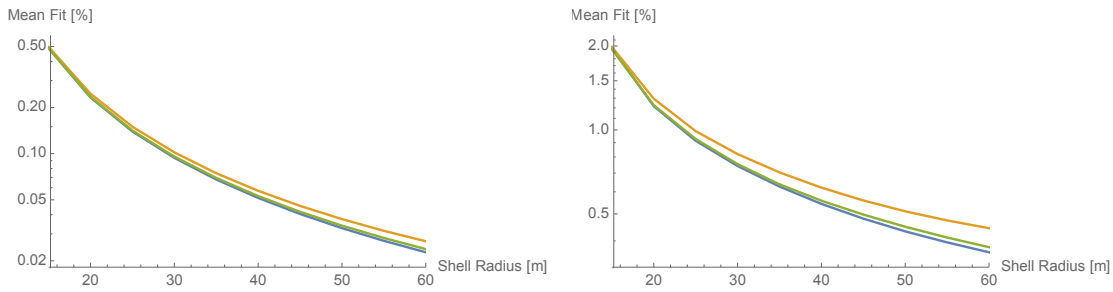

(a) Force Errors

(b) Torque Errors

Figure 13. 4DOF Force and Torque Error Comparison, (—) Three-Sphere Model Three Whole Shells, (—) Three-Sphere Model One Half Shell, (—) Three-Sphere Model One Whole Shell (4DOF)

Table 5. Total Function Calls for 4DOF Model Comparison

Model	Total Function Calls
4DOF	1471866
3DOF 3 Shells	2640779
3DOF 1 Half Shell	875643

to one half shell of data. The 4DOF model's accuracy resembles the 3DOF model fitted to three whole shells. Since the optimizer knows nothing about the symmetry of the box-and-panel model, a whole shell of data must be used to generate an accurate model when 4DOF is used. Total function calls for each of the models shown in Figure 13 are shown in Table 5. Surprisingly, the 4DOF modeling method results in nearly half the function calls of the 3DOF three shell or 3DOF one 15 m shell models. Unsurprisingly, the best model from a computation perspective is the 3DOF one half shell model. These results show that 4DOF modeling using E-field fitting is promising from both an accuracy and performance perspective.

FUTURE WORK

The ultimate test of this fitting method is a comparison between the generated VMSM model forces and torques and numerically generated force and torque data from FEM software. SMSM models produce very accurate force and torque data when compared to Maxwell 3D, and it is promising that the E-field fitting technique produces VMSM models that not only match a SMSM model's electric field to high accuracy, but also match SMSM predicted forces and torques. Nevertheless, future research will be conducted to verify that VMSM models generated using electric field fitting do match FEM data to high accuracy.

The performance of the E-field matching method suggests that the results of the cost function analysis can be extrapolated to higher dimension search spaces; however, more research into the convergence properties of the E-field fitting technique should be carried out. Although a self-capacitance constraint is imposed in this work, other appropriate constraints might be found to further reduce the dimension of the search space and aid performance. Research into the convergence properties of the E-field matching method might lead the way to fully autonomous model generation using 4DOF VMSM models.

The selected target geometry represents a particular target of interest that might be found at GEO. The box-and-panel target geometry is not representative of all objects of interest, and VMSM modeling of more complicated geometries should be investigated. These geometries should be selected to represent a healthy cross section of potential targets at GEO. An assumption is made in this work that the target is a perfect conductor, but many objects of interest have dielectric properties. Extension of this work to model dielectrics is a worthwhile pursuit.

CONCLUSION

Using E-field matching and VMSM sphere populations provides highly accurate fits with respect to SMSM models with lower computational burden than previously explored methods. The presented E-field matching fits to smooth, analytically generated data, does not rely on probe geometry and has a simpler cost function that easily leverages self-capacitance constraints to increase computational efficiency, improve force and torque fits far from a target and reduce the amount of data required for optimization. The improvements with E-field matching over previously studied methods is apparent int he more rapid convergence of two and three-sphere VMSM models of a box-and-panel spacecraft. The proposed E-field matching method provides a more suitable approach for complicated spacecraft geometries and higher degree-of-freedom optimizations due to reduced computational time and improved fit accuracy. E-field matching provides a fast and simple means of generating VMSM models for electrostatic modeling of spacecraft and debris.

ACKNOWLEDGMENT

This research is funded through a grant No. FA9550-15-1-0407 from the Air Force Office of Space Research.

REFERENCES

[1] P. Chow, J. Hughes, T. Bennett, and H. Schaub, "Automated Sphere Geometry Optimization for the Volume Multi-Sphere Method," *AAS/AIAA Space Flight Mechanics Meeting*, No. AAS-16-672, Napa Valley, California, Feb. 14–18 2016.

[2] S. N. Paul and C. Frueh, *Space Debris Charging and its Effect on Orbit Evolution*. American Institute of Aeronautics and Astronautics, 2016.

[3] C. Früh, D. Ferguson, C. Lin, and M. Jah, "The Effect of Passive Electrostatic Charging on Near-Geosynchronous High Area-To-Mass Ratio Objects," *International Astronautical Congress*, Vol. 64, 2013.

[4] J. Hughes and H. Schaub, "Charged Geosynchronous Debris Perturbation Using Rapid Electromagnetic Force and Torque Evaluation," *Advanced Maui Optical and Space Surveillance Technologies Conference*, Maui, Hawaii, Sep. 20–23 2016.

[5] M. A. Peck, "Prospects and Challenges for Lorentz-Augmented Orbits," *AIAA Guidance, Navigation and Control Conference*, San Francisco, CA, August 15–18 2005. Paper No. AIAA 2005-5995.

[6] H. Schaub and Z. Sternovsky, "Active Space Debris Charging for Contactless Electrostatic Disposal Maneuvers," *6th European Conference on Space Debris*, Darmstadt, Germany, ESOC, April 22–25 2013. Paper No. 6b.O-5.

[7] T. Bennett, D. Stevenson, E. Hogan, L. McManus, and H. Schaub, "Prospects and Challenges of Touchless Debris Despinning Using Electrostatics," *Advances in Space Research*, Vol. 56, Aug. 2015, pp. 557–568, 10.1016/j.asr.2015.03.037.

[8] M. A. Peck, B. Streetman, C. M. Saaj, and V. Lappas, "Spacecraft Formation Flying using Lorentz Forces," *Journal of British Interplanetary Society*, Vol. 60, July 2007, pp. 263–267.

[9] L. A. Sobiesiak and C. J. Damaren, "Lorentz-Augmented Spacecraft Formation Reconfiguration," *AIAA/AAS Astrodynamics Specialist Conference*, San Diego, California, Aug. 4–7 2014.

[10] B. Streetman and M. A. Peck, "General Bang-Bang Control Method for Lorentz Augmented Orbits," *Journal of Spacecraft and Rockets*, Vol. 47, May–June 2010, pp. 484–492, 10.2514/1.45704.

[11] E. A. Hogan and H. Schaub, "General High-Altitude Orbit Corrections Using Electrostatic Tugging with Charge Control," *Journal of Guidance, Control, and Dynamics*, Vol. 28, April 2015, pp. 699–705, 10.2514/1.G000092.

[12] E. Hogan and H. Schaub, "Relative Motion Control for Two-Spacecraft Electrostatic Orbit Corrections," *AIAA Journal of Guidance, Control, and Dynamics*, Vol. 36, Jan. – Feb. 2013, pp. 240–249.

[13] H. Schaub and D. F. Moorer, "Geosynchronous Large Debris Reorbiter: Challenges and Prospects," *AAS Kyle T. Alfriend Astrodynamics Symposium*, Monterey, CA, May 17–19 2010. Paper No. AAS 10-311.

[14] T. Bennett and H. Schaub, "Touchless Electrostatic Detumbling While Tugging Large Axi-Symmetric GEO Debris," *AAS/AIAA Space Flight Mechanics Meeting*, Williamsburg, VA, Jan. 11–15 2015. Paper AAS 15-383.

[15] T. Bennett and H. Schaub, "Touchless Electrostatic Three-Dimensional Detumbling of Large Axi-Symmetric Debris," *Journal of Astronautical Sciences*.

[16] H. Schaub, T. Bennett, and J. Hughes, "Current Developments in Three-Dimensional Electrostatic Detumble of Axi-Symmetric GEO Debris," *4th International Workshop on Space Debris Modeling and Remediation, CNES*, Paris, June 6–8 2016. Paper No. 6.4.

[17] D. Stevenson and H. Schaub, "Multi-Sphere Method for Modeling Electrostatic Forces and Torques," *Advances in Space Research*, Vol. 51, Jan. 2013, pp. 10–20, 10.1016/j.asr.2012.08.014.

[18] D. Stevenson, "Optimization of Sphere Population for Electrostatic Multi Sphere Model," *12th Spacecraft Charging Technology Conference*, Kitakyushu, Japan, May 14–18 2012.

[19] W. R. Smythe, *Static and Dynamic Electricity*. McGraw–Hill, 3rd ed., 1968.

[20] W. C. Gibson, *The Method of Moments in Electromagnetics*. Chapman & Hall, November 28 2007.

[21] H. Schaub, "Faster-than-Realtime Electrostatic Force and Torque Modeling for SSA Applications," AFOSR Annual Report, University of Colorado, Aerospace Engineering Sciences Department, Boulder, CO, September 14 2016.

[22] J. Maxwell, *A Treatise on Electricity and Magnetism*. Oxford University Press, 1893.

[23] J. Lekner, "Electrostatics of two charged conducting spheres," *Procedings of the Royal Society*, Vol. 468, 2012, pp. 2829–2848.

[24] R. Bauer, "Distribution of Points on a Sphere with Application to Star Catalogs," *Journal of Guidance Control and Dynamics*, Vol. 23, No. 1, 2000, pp. 130–137.